Supporting Information for

# Computational mining of GeH-based Janus III–VI van der Waals heterostructures for solar cell applications

Ruifeng Li[a], Zhichao Shi[a], Rui Xiong[a], Zhou Cui[a], Yinggan Zhang[b], Chao Xu[c], Jingying Zheng[a], Bo Wu[a], Baisheng Sa[a,*] and Cuilian Wen[a,**]

[a] *Multiscale Computational Materials Facility, and Key Laboratory of Eco-materials Advanced Technology, College of Materials Science and Engineering, Fuzhou University, Fuzhou 350100, P. R. China*

[b] *College of Materials, Fujian Provincial Key Laboratory of Theoretical and Computational Chemistry, Xiamen University, Xiamen 361005, P. R. China*

[c] *Xiamen Talentmats New Materials Science & Technology Co., Ltd., Xiamen 361015, P. R. China*

**Corresponding Authors:** bssa@fzu.edu.cn (B. Sa), clwen@fzu.edu.cn (C. Wen).

**Table S1.** The energy differences of $\Delta E$ (meV) and interlayer distance $d$ (Å) as well as the lattice constants $a$ (Å) for heterostructures

| System | Configuration | $\Delta E$ | $d$ | $a$ |
|---|---|---|---|---|
| $Ga_2SeTe$/GeH | d | 77 | 3.155 | 4.000 |
| | e | 0 | 2.359 | 4.007 |
| | f | 3 | 2.282 | 4.011 |
| $In_2SSe$/GeH | d | 82 | 2.965 | 4.011 |
| | e | 4 | 2.160 | 4.017 |
| | f | 0 | 2.038 | 4.023 |
| $In_2STe$/GeH | d | 85 | 3.112 | 4.087 |
| | e | 0 | 2.277 | 4.096 |
| | f | 5 | 2.223 | 4.100 |
| $In_2SeTe$/GeH | d | 88 | 3.138 | 4.126 |
| | e | 0 | 2.221 | 4.135 |
| | f | 3 | 2.195 | 4.141 |

**Table S2.** The electron gains of the isolated $In_2STe$ $\sum P_{In_2STe}$ $(e)$, and GeH monolayers $\sum P_{GeH}$ $(e)$ based on different methods

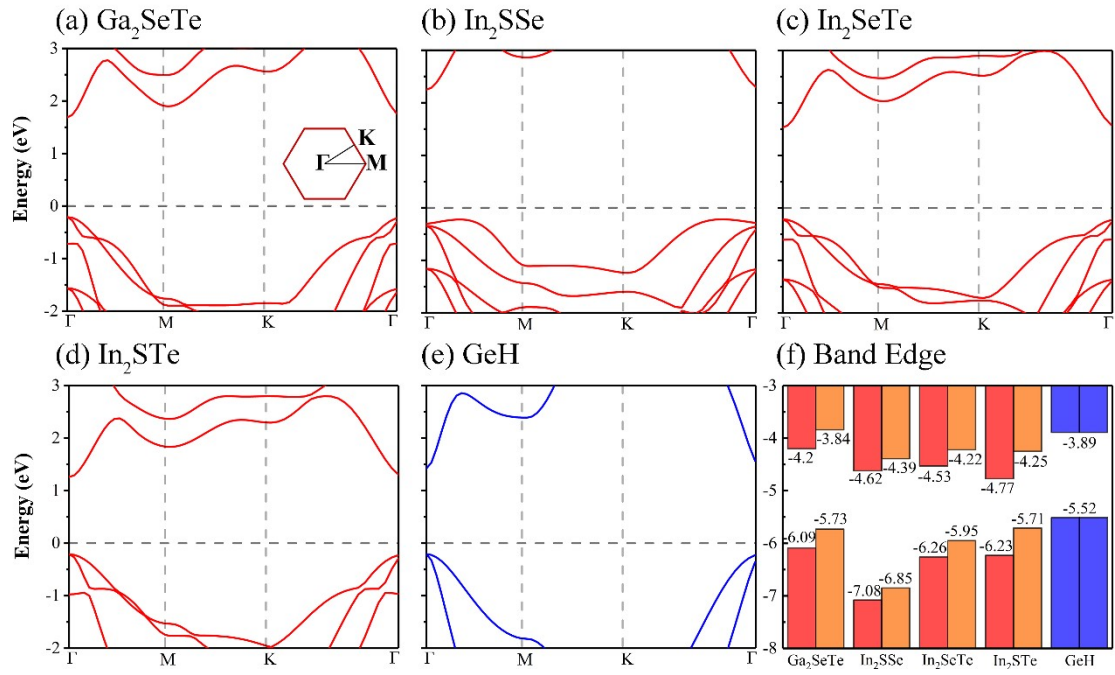| Method | $\sum P_{GeH}$ | $\sum P_{In_2STe}$ |
|---|---|---|
| Differential Charge Densities | 0.000019 | -0.000019 |
| Bader Charge | 0.012 | -0.012 |

**Figure S1.** HSE06 band structures of (a) Ga$_2$SeTe, (b) In$_2$SSe, (c) In$_2$SeTe, (d) In$_2$STe and (e) GeH monolayers. The first Brillouin zone with high-symmetry points is shown in the inset of (a). (l) The band edge alignments for the monolayers. The red pillars indicate the band edge alignments of the X side, and the orange pillars indicate the band edge alignments of the Y side.
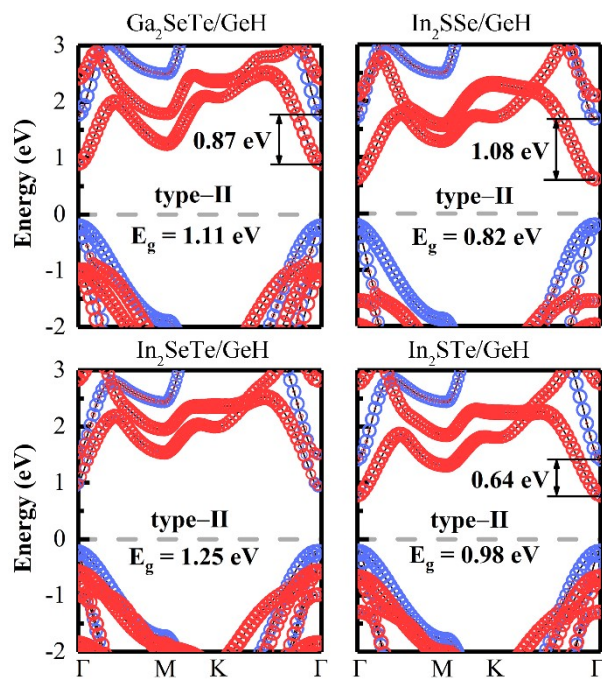
**Figure S2.** Projected HSE06 band of the most stable $M_2XY$/GeH vdW heterostructures among configurations (a) to (c). Red and blue circles represent the projected weights of $M_2XY$ and GeH monolayers, respectively.
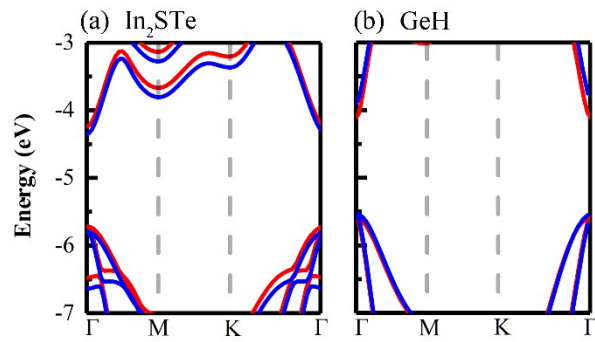
**Figure S3.** HSE06 band structures of (a) In$_2$SeTe and (b) GeH monolayers. Red and blue curves represent the band structures for intrinsic monolayers and the mutually independent monolayers fixed in the lattice of In$_2$STe/GeH vdW heterostructure, respectively.
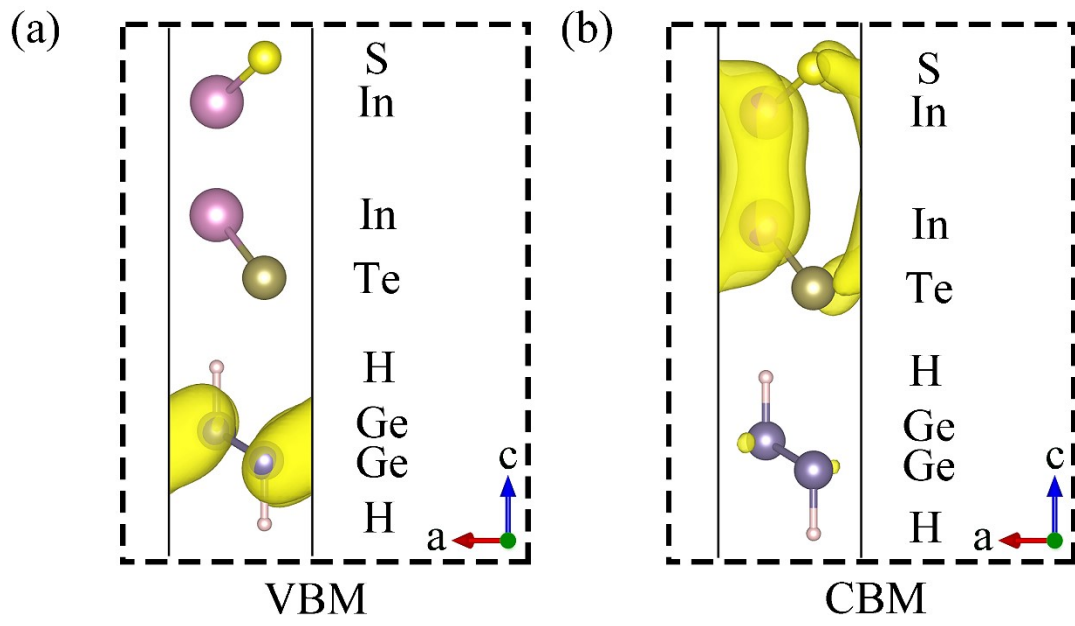
**Figure S4.** Band-decomposed charge density of the (a) VBM and (b) CBM for In$_2$STe/GeH heterostructure.

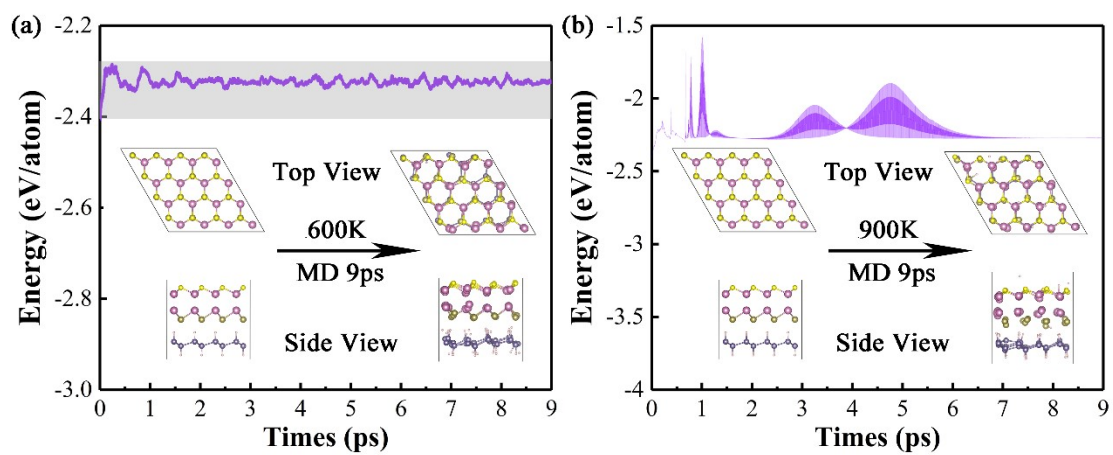**Figure S5.** Total energy changes and structure snapshots from AIMD calculations at (a) 600 K and (b) 900 K of In$_2$STe/GeH vdW heterostructure.

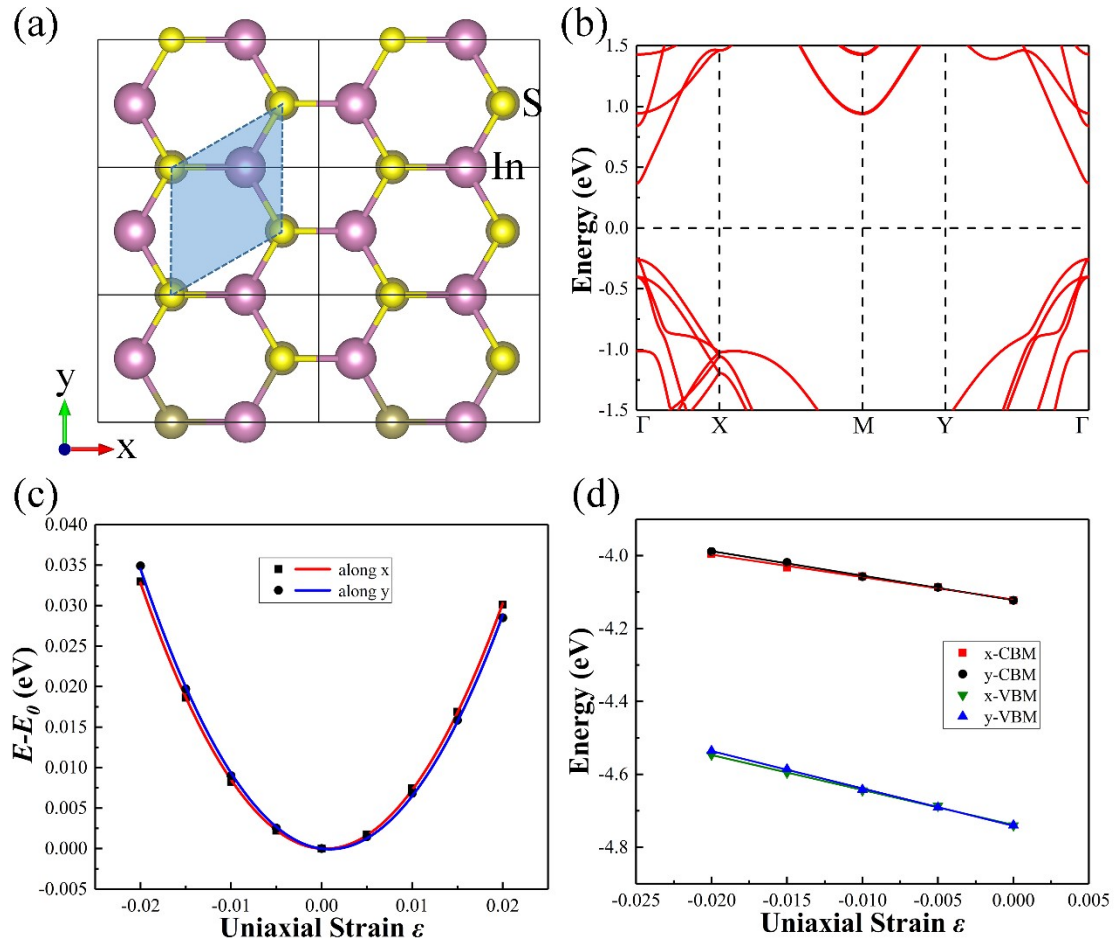**Figure S6.** (a) Using an orthorhombic lattice to calculate In$_2$STe/GeH vdW heterostructure and the blue shaded quad indicates the initial hexagonal lattice. (b) Band structure of In$_2$STe/GeH vdW heterostructure by the PBE method. (c) Total energy shift $E - E_0$ and (d) Band edge positions of In$_2$STe/GeH vdW heterostructure as functions of the uniaxial strain $\varepsilon$ along with both the armchair ($x$) and zigzag ($y$) directions by the PBE method. The vacuum level is set to 0 for reference in (d) figure.